International Journal of Thermophysics, Vol. 19, No. 5, 1998

Subcritical and Supercritical Water Radial Distribution Function

H. Touba,[1] G. A. Mansoori,[1,2] and E. Matteoli[3]

Received December 3, 1997

A theoretical and analytic expression for the first shell, and an analytic empirical expression for the whole radial distribution function (RDF) of water are introduced. All the asymptotic limits and functionalities of the RDF with temperature and density are incorporated in these expressions. An effective Kihara pair potential function is presented for water intermolecular interactions which incorporates the hydrogen bonding by using the chain association theory. The intermolecular pair potential parameters are adjusted to the experimental x-ray diffraction data of water RDF at various temperatures. The predicted first-shell results for water near critical and in supercritical conditions compare satisfactorily with the available neutron diffraction RDF data, with the simulation RDF results, and with the empirical RDF curves. The empirical expression initially proposed for the RDF of the Lennard–Jones fluid is extended to predict the RDF and the isothermal compressibility of water to conditions where experimental or simulated data are not available. Comparison with the Lennard–Jones fluid shows that the height of the first peak of water RDF changes much less at subcritical and supercritical conditions compared to that of the Lennard–Jones fluid which decreases appreciably going from subcritical to supercritical conditions.

KEY WORDS: Kihara energy function; radial distribution function; water; supercritical fluid.

1. INTRODUCTION

Over the last two decades, there have been extensive studies to explore the detailed structural behavior of water. The molecular structure and macroscopic properties of water in various phases have been studied and

[1] Department of Chemical Engineering, University of Illinois at Chicago, 810 S. Clinton, Chicago, Illinois 60607-7000, U.S.A.

[2] To whom correspondence should be addressed.

[3] Istituto di Chimica Quantistica ed Energetica Molecolare, 56100 Pisa, Via Risorgimento 35, Italy.

0195-928X/98/0900-1447$15.00/0

measured carefully, and the related data are compiled since the nineteenth century. However, our understanding of the statistical-mechanical relations between microscopic and macroscopic behaviors of water is still limited and inaccurate.

The radial distribution function (RDF) of water is the most informative feature of its molecular structure, and its knowledge over wide ranges of pressure and temperature joined with an appropriate potential function would allow a detailed understanding of the structure and prediction of properties (such as solubility and phase equilibria) not only for the pure substance but also for mixtures. Particularly important would be this knowledge near the critical conditions, because of the wide industrial application of water as an extracting solvent.

Recently Touba and Mansoori [1] proposed a functional form for the first shell of the RDF which was applied to the Lennard–Jones and Kihara potential energy functions. This model has produced results in good agreement with the available computer simulation data of RDF for these model fluids and the experimental data for argon. As a continuation of the above study on the RDF of fluids, it is deemed interesting to extend this model to water from normal to supercritical conditions. To achieve this purpose, an effective Kihara pair potential is derived for water molecules which incorporates the hydrogen bonding according to the analytic chain association theory and the conformal solution theory.

In order to check the reliability of this model in various conditions, we have also extended the application of another expression for the total RDF curve to extrapolate the features of the experimental RDF of water. This model which was proposed initially for the prediction of Lennard–Jones fluid RDF by Matteoli and Mansoori [2] produces accurate values for the isothermal compressibility of water.

2. THE FIRST-SHELL RADIAL DISTRIBUTION FUNCTION MODEL FOR WATER

Two limiting conditions that the RDF has to satisfy are the case of dilute gases in which the density approaches zero and the case of hard spheres, where the temperature approaches infinity. The RDF of dilute gases can be derived from statistical thermodynamics as:

$$g_{dg}(y) = \exp[-\beta\phi(y)] \tag{1}$$

where $g_{dg}(y)$ is the dilute gas RDF, $y \equiv r/\sigma$, r is the intermolecular distance, σ is the length parameter in the potential energy function, ϕ is the inter-

molecular potential energy function, $\beta = 1/(kT)$, T is the absolute temperature, and k is Boltzmann's constant.

Touba and Mansoori [1] proposed the following functional form for the first shell of the RDF which satisfies these two limiting cases.

$$g(y) = m_1 g_{\text{hs}}(1) \exp[-m_2 \beta\phi(x)] + (1 - m_1) \exp[-m_2 \beta\phi(y) - c_1(y - d^*)]$$
$$\text{for} \quad 0 \leqslant y \leqslant d^* \tag{2}$$

$$g(y) = m_1 g_{\text{hs}}(x) + (1 - m_1) \exp[-m_2 \beta\phi(y) - c_2(y - d^*)]$$
$$\text{for} \quad d^* \leqslant y \leqslant y_m \tag{3}$$

where $x \equiv r/d$, $d^* \equiv d/\sigma$, d is the location of maximum of RDF which in the case of hard sphere RDF corresponds to the hard-core diameter, y_m is the minimum of the RDF after the first peak, and $g_{\text{hs}}(x)$ is the hard sphere RDF for which Wertheim's analytical solution [3] of the Percus–Yevick equation for the first shell of hard sphere RDF has been utilized. Both Eqs. (2) and (3) converge to the following simple equation at the maximum of the first peak of the RDF (at $y = d^*$).

$$g(d^*) = m_1 g_{\text{hs}}(1) + (1 - m_1) \exp[-m_2 \beta\phi(d^*)] \tag{4}$$

The parameters c_1 and c_2 appearing in Eqs. (2) and (3) must be determined from the fact that the $g(y)$ has to be maximum at distance d^*, i.e., $[\partial g(y)/\partial y]_{y=d^*} = 0$.

$$c_1 = -m_1 m_2 \beta\phi'(1)\, g_{\text{hs}}(1)/\{d^*(1 - m_1) \exp[-m_2 \beta\phi(d^*)]\}$$
$$- m_2 \beta\phi'(d^*) \tag{5}$$

$$c_2 = m_1 g'_{\text{hs}}(1)/\{d^*(1 - m_1) \exp[-m_2 \beta\phi(d^*)]\} - m_2 \beta\phi'(d^*) \tag{6}$$

The parameters m_1, m_2, and d^* in the RDF equation are expressed as functions of the dimensionless temperature $T \equiv kT/\varepsilon$, ε being the energy parameter of the potential energy function, and dimensionless density $\rho^* = \rho\sigma^3$ in such a way that they satisfy the limiting conditions of RDF:

$$m_1 = \exp[-4.93/(\rho^* T^*)] \tag{7}$$

$$m_2 = \exp[0.68\rho^*(1 - 1/T^*)] \tag{8}$$

$$d^* = R_m \exp(-0.0483 \rho^{*2} T^{*0.5}) \tag{9}$$

R_m is the location of the dilute gas RDF peak which can be calculated by solving the following equation:

$$[\partial\phi(y)/\partial y]_{y=R_m} = \phi'(y = R_m) = 0 \tag{10}$$

According to Eq. (7), as the temperature approaches infinity, m_1 will approach unity. Therefore, we conclude that Eq. (3) approaches the limiting case of the hard sphere RDF, g_{hs}, for $y \geqslant d^*$ (or $x \geqslant 1$). For the case where the density is very low, according to Eqs. (5)–(10), $m_1 = c_1 = c_2 = 0$ and $m_2 = 1$. Therefore, Eqs. (2) and (3) reduce to Eq. (1), the dilute gas RDF.

The above expressions have initially been applied to simple potential energy functions, such as the Lennard–Jones and Kihara [1]. By using the analytic chain association theory and the conformal solution theory, it is possible to derive an effective Kihara pair potential function for water which incorporates the hydrogen bonding. This effective potential function can then be introduced into the above expressions in order to predict the first shell RDF of water.

3. AN EFFECTIVE KIHARA PAIR POTENTIAL FUNCTION FOR WATER

The Kihara pair potential energy function assumes that each molecule has an impenetrable hard core of diameter δ and accounts for the intermolecular forces.

$$\phi(y) = 4\varepsilon\{[(1-\delta^*)/(y-\delta^*)]^{12} - [(1-\delta^*)/(y-\delta^*)]^6\} \tag{11}$$

where $\delta^* \equiv \delta/\sigma$. In order to use the Kihara potential function in the first-shell RDF model previously presented, we need to derive the expressions for $\phi(x)$, $\phi(d^*)$, $\phi'(d^*)$, $\phi'(1)$, and R_m, as determined below:

$$\phi(x) = 4\varepsilon\{[(1-\delta^*/d^*)/(x-\delta^*/d^*)]^{12} - [(1-\delta^*/d^*)/(x-\delta^*/d^*)]^6\} \tag{12}$$

$$\phi(d^*) = 4\varepsilon\{[(1-\delta^*)/(d^*-\delta^*)]^{12} - [(1-\delta^*)/(d^*-\delta^*)]^6\} \tag{13}$$

$$\phi'(d^*) = [-24\varepsilon/(d^*-\delta^*)] \times \{2[(1-\delta^*)/(d^*-\delta^*)]^{12} - [(1-\delta^*)/(d^*-\delta^*)]^6\} \tag{14}$$

$$\phi'(1) = -24\varepsilon/(1-\delta^*/d^*) \tag{15}$$

$$R_m = \delta^* + 2^{1/6}(1-\delta^*) \tag{16}$$

The key feature of water intermolecular energy is the hydrogen bonding which brings about formation of chemical aggregates or polymers. In order to reproduce the intermolecular characteristics of water, the hydrogen bonding has to be assimilated into the Kihara potential function

parameters. Several investigators have suggested that some form of hydrogen bonding is present even at supercritical conditions [4–6]. Nemethy and Scherga [7] indicated through their studies on water structure that hydrogen bonding plays an important role in forming aggregates that can reach sizes of up to one hundred H_2O molecules at room temperature. We represent the association of water molecules due to hydrogen bonding with the following chain reaction [8].

$$(H_2O)_i + (H_2O)_1 \overset{K_i(T)}{\Longleftrightarrow} (H_2O)_{i+1} \qquad i = 1, 2, \ldots, \infty \tag{17}$$

Assuming that the associating species form an ideal solution, we can express the equilibrium constant of the above reaction as:

$$K_i = x_{i+1}/(x_i x_1) \qquad i = 1, 2, \ldots, \infty \tag{18}$$

where x_i is the mole fraction of $(H_2O)_i$. For simplicity we assume that all K_i's are the same, (i.e., $K = K_1 = K_2 = \cdots = K_i = \cdots$).

We may extend Eq. (18) to different associating species as follows:

$$\begin{aligned} x_2 &= Kx_1^2 \\ x_3 &= Kx_2x_1 = K^2x_1^3 \\ x_4 &= Kx_3x_1 = K^3x_1^4 \\ &\vdots \\ x_{i+1} &= Kx_ix_1 = K^ix_1^{i+1} \\ &\vdots \end{aligned} \tag{19}$$

By using the above system of equations, x_i's may be calculated provided that x_1 and K are known. Since summation of all mole fractions is unity, then

$$x_1 + Kx_1^2 + K^2x_1^3 + \cdots + K^ix_1^{i+1} + \cdots = 1$$

$$\sum_{i=0} K^ix_1^{i+1} = 1 \tag{20}$$

Considering $Kx_1 < 1$, we may show that the series on the left side of Eq. (20) converges to

$$x_1/(1 - Kx_1) = 1 \tag{21}$$

Then, the following relation will result from Eq. (21).

$$x_1 = 1/(1+K) \tag{22}$$

Having a large number of associated species, compositions may be replaced with a composition distribution function $\chi(I)$ where I is the number of associated monomers. In this case, the summation in Eq. (20) can be replaced with an integral.

$$\int_0^\infty \chi(I)\, dI = 1 \tag{23}$$

where $\chi(I)$ is defined as follows:

$$\chi(I) \equiv \chi_0 K^I x_1^{I+1} \tag{24}$$

χ_0 is the normalizing factor and can be calculated by using Eq. (23).

$$\chi_0 = -(\ln Kx_1)/x_1 \tag{25}$$

By joining Eqs. (22), (24), and (25) we get the following result:

$$\chi(I) = -[K/(1+KK)]^I \ln[K/(1+K)] \tag{26}$$

The association constant, K, appearing in this equation is generally expressed as:

$$\ln K = (T\,\Delta S^\circ - \Delta H^\circ)/(RT) \tag{27}$$

where the reference changes of enthalpy and entropy of association, ΔH° and DS°, are independent of temperature. The most reliable values for ΔH° and ΔS° are those obtained by using spectroscopic methods, such as Raman spectroscopy as reported in Ref. 9:

$$\Delta H^\circ = -22\ \text{kJ} \cdot \text{mol}^{-1}, \qquad \Delta S^\circ = -52\ \text{J} \cdot \text{mol}^{-1} \cdot \text{K}^{-1}$$

Applying the conformal solution theory, which assumes that there exists a pure hypothetical fluid with the same properties as those of the mixture at the same density and temperature, the pair potential Φ_{ij} can be represented as follows [10]:

$$\Phi_{ij} = \varepsilon_{ij}\, \Phi_{00}(r/\sigma_{ij}) \tag{28}$$

where the subscript (00) denotes the reference fluid and the parameters σ_{ij} and ε_{ij} represent the molecular conformal diameter and energy parameters,

respectively. The conformal solution theory is considered quite effective in extending the applicability from pure fluids to fluid mixtures. Among the statistical mechanical conformal solution theories of mixtures, the one-fluid van der Waals theory is simple to use and accurate enough [11] with the following form for the parameters of the Kihara potential.

$$\sigma^3 = \sum_i \sum_j x_i x_j \sigma_{ij}^3 \tag{29}$$

$$\varepsilon\sigma^3 = \sum_i \sum_j x_i x_j \varepsilon_{ij} \sigma_{ij}^3 \tag{30}$$

$$\delta^3 = \sum_i \sum_j x_i x_j \delta_{ij}^3 \tag{31}$$

Applying the combining rules $\sigma_{ij}^3 = (\sigma_i^3 + \sigma_j^3)/2$, $\delta_{ij}^3 = (\delta_i^3 + \delta_j^3)/2$, and $\varepsilon_{ij} = (\varepsilon_i \varepsilon_j)^{1/2}$ for the unlike-interaction potential parameters, we get the following expressions:

$$\sigma^3 = \sum_i \sum_j x_i x_j [(\sigma_i^3 + \sigma_j^3)/2] = \sum_i x_i \sigma_i^3 \tag{32}$$

$$\delta^3 = \sum_i \sum_j x_i x_j [(\delta_i^3 + \delta_j^3)/2] = \sum_i x_i \delta_i^3 \tag{33}$$

$$\begin{aligned} \varepsilon\sigma^3 &= \sum_i \sum_j x_i x_j (\varepsilon_i \varepsilon_j)^{1/2} [(\sigma_i^3 + \sigma_j^3)/2] \\ &= \sum_i (x_i \varepsilon_i^{1/2} \sigma_i^3) \sum_j x_j \varepsilon_j^{1/2} \end{aligned} \tag{34}$$

Considering the number of associating species to be very large, we can replace the above summations with integrals and the compositions with the composition distribution function which was already derived.

$$\sigma^3 = \int_0^\infty \chi(I)[\sigma(I)]^3 \, dI \tag{35}$$

$$\delta^3 = \int_0^\infty \chi(I)[\delta(I)]^3 \, dI \tag{36}$$

$$\varepsilon\sigma^3 = \int_0^\infty \chi(I)[\varepsilon(I)]^{1/2} [\sigma(I)]^3 \, dI \int_0^\infty \chi(I)[\varepsilon(I)]^{1/2} \, dI \tag{37}$$

We relate parameters $[\sigma(I)]^3$, $[\delta(I)]^3$, and $[\varepsilon(I)]^{1/2}$ to the following functions of the distribution index "I".

$$[\sigma(I)]^3 = \sigma_1^3 I^{\xi_1} \tag{38}$$

$$[\delta(I)]^3 = \delta_1^3 I^{\xi_2} \tag{39}$$

$$[\varepsilon(I)]^{1/2} = \varepsilon_1^{1/2} I^{\xi_3}[1 + \xi_3(1/I - 1) + \xi_4(1 - I)] \tag{40}$$

where σ_1, δ_1, and ε_1 are the potential energy function parameters for the monomer and ξ_1, ξ_2, ξ_3, and ξ_4 are constants.

Substituting Eqs. (26) and (38) to (40) into Eqs. (35) to (37), respectively, and integrating, we will have:

$$\sigma = \sigma_1[\Gamma(1 + \xi_1)\,\theta^{\xi_1}]^{1/3} \tag{41}$$

$$\delta = \delta_1[\Gamma(1 + \xi_2)\,\theta^{\xi_2}]^{1/3} \tag{42}$$

$$\begin{aligned}\varepsilon = {} & \varepsilon_1 \theta^{2\xi_3}[\Gamma(1 + \xi_1 + \xi_3)\,\Gamma(1 + \xi_3)/\Gamma(1 + \xi_1)] \\ & \times \{1 + \xi_3/[(\xi_1 + \xi_3)\,\theta] - \xi_3 + \xi_4[1 - (2 + \xi_1 + \xi_3)\,\theta]\} \\ & \times \{1 + 1/\theta - \xi_3 + \xi_4[1 - (2 + \xi_3)\theta]\}\end{aligned} \tag{43}$$

where Γ is the gamma function and θ is defined as:

$$\theta \equiv -1/\ln[K/(1 + K)]$$

Equations (41) to (43) when joined with the Kihara potential energy function, Eq. (11), represent the effective intermolecular potential energy function for an associating fluid, such as water. The Kihara parameters for water have been calculated by using the proposed expressions for the first shell of the RDF and the experimental data reported by Narten and Levy [12]. Figures 1–3 show the variations of calculated values of σ, δ, and ε for the Kihara potential function with temperature.

According to Fig. 1, it can be seen that σ does not practically change with temperature which implies that in Eq. (41), we can assume $\xi_1 = 0$ which results in:

$$\sigma = \sigma_1 = 2.68 \text{ Å} \tag{44}$$

According to Fig. 2, the δ parameter of the Kihara potential for water is a decreasing function of temperature. The values of ξ_2 and δ_1 appearing in Eq. (42) are found to be $\xi_2 = 1.0$ and $\delta_1 = 0.35$ Å by fitting the data of this figure to Eq. (42). Hence Eq. (42) becomes

$$\delta = 0.35\,\theta^{1/3} \tag{45}$$

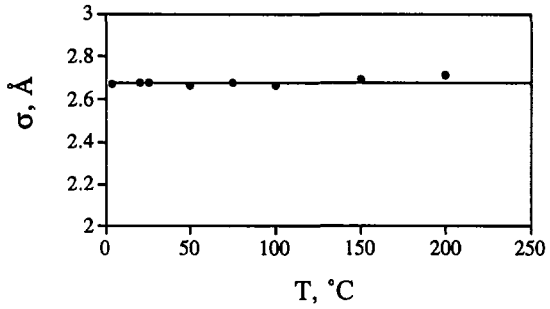

Fig. 1. Variations of σ with temperature using the proposed equation for the first shell of RDF.

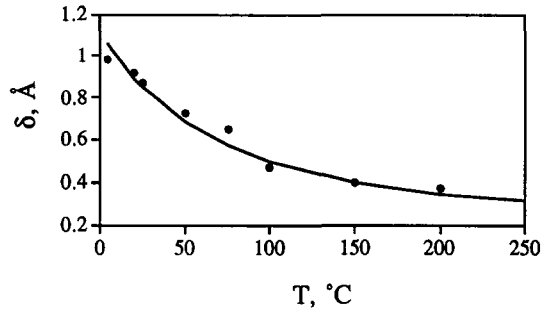

Fig. 2. Variations of δ with temperature using the proposed equation for the first shell of RDF.

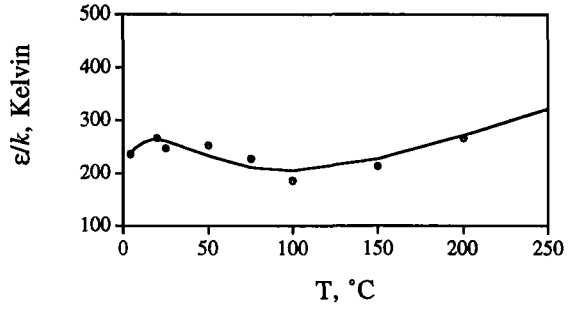

Fig. 3. Variations of ε with temperature using the proposed equation for the first shell of RDF.

According to Fig. 3, the variation of ε/k with temperature is not monotonic. Since $\xi_1 = 0$ then Eq. (43) can be simplified to the following form:

$$\varepsilon = \varepsilon_1 \{\theta^{\xi_3} \Gamma(1+\xi_3)\{1 + 1/\theta - \xi_3 + \xi_4[1-(2+\xi_3)\theta]\}\}^2 \tag{46}$$

By fitting this equation to the data of ε/k versus temperature in Fig. 3, it is shown that these data can be best represented by Eq. (46) when $\varepsilon_1/k = 130$ K, $\xi_3 = 0.4$, and $\xi_4 = 0.0036$.

In Figs. 1–3, the circles represent the experimental data and the solid lines represent the calculations by Eqs. (44)–(46). According to these figures, these correlations are in very good agreement with the experimental data.

4. CALCULATIONS AND COMPARISONS

The molecular structure of water has conventionally been characterized with the RDF data which are available either from x-ray diffraction and neutron scattering experiments or from computer simulations. The proposed RDF expressions along with the corresponding water potential energy function have been tested versus the experimental and simulation data.

Figures 4–11 represent the calculated first shell of the RDF of water at temperatures 4, 20, 25, 50, 75, 100, 150, and 200°C, respectively. The

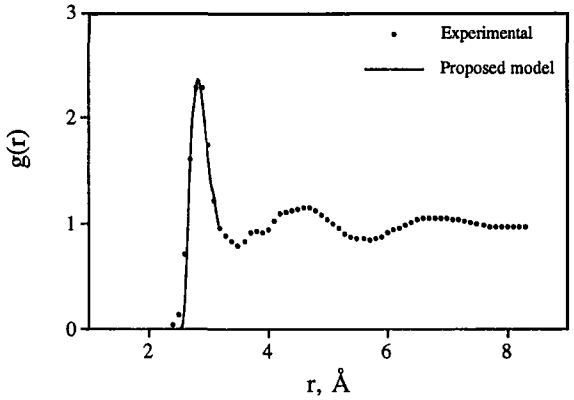

Fig. 4. Comparison of the proposed model for the first shell of RDF and the experimental data (Narten and Levy [12]) at $T = 4$°C.

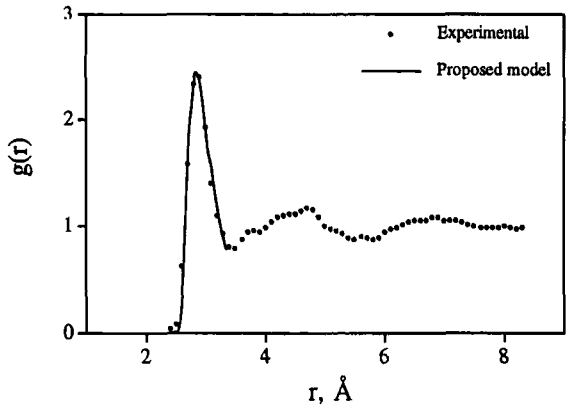

Fig. 5. Comparison of the proposed model for the first shell of RDF and the experimental data (Narten and Levy [12]) at $T = 20°C$.

effective Kihara potential function has been used for associating fluids as derived and reported in the previous section. Also reported in these figures are the experimental data of the water RDF by Narten and Levy [12]. According to these figures, predictions of the first shell by the proposed model are in excellent agreement with the experimental data.

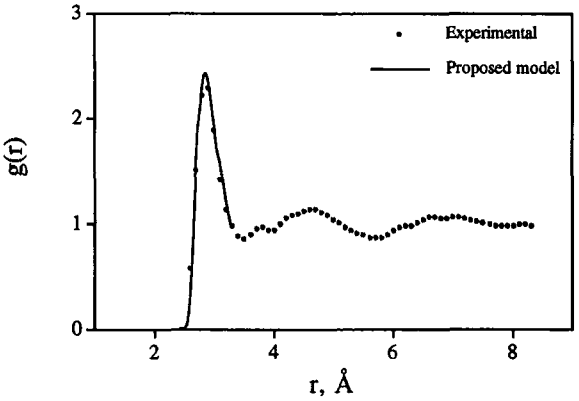

Fig. 6. Comparison of the proposed model for the first shell of RDF and the experimental data (Narten and Levy [12]) at $T = 25°C$.

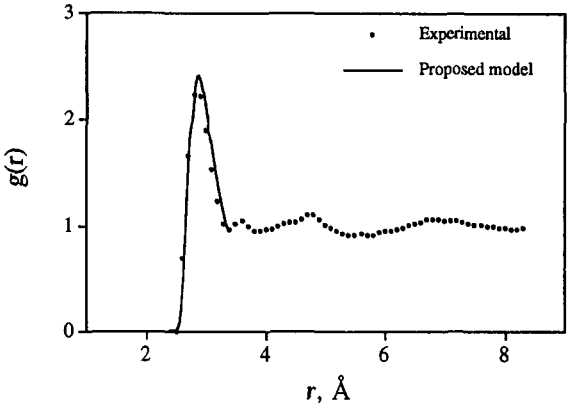

Fig. 7. Comparison of the proposed model for the first shell of RDF and the experimental data (Narten and Levy [12]) at $T = 50°C$.

Experimental data of water RDF at near-critical conditions are not numerous. However, it would be interesting to examine if the present model is able to predict reliable RDF values at these conditions. To do that, we have considered the following equations for the complete RDF of Lennard–Jones fluids proposed by Matteoli and Mansoori [2], and used

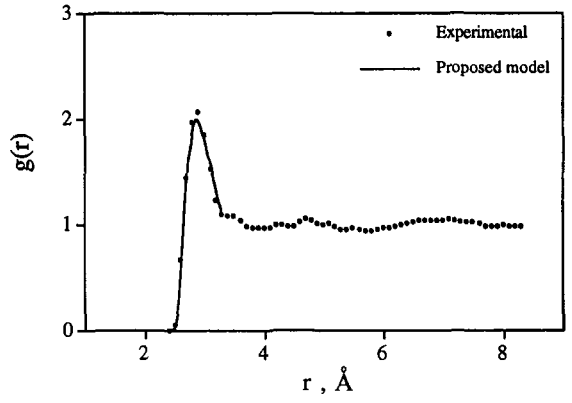

Fig. 8. Comparison of the proposed model for the first shell of RDF and the experimental data (Narten and Levy [12]) at $T = 75°C$.

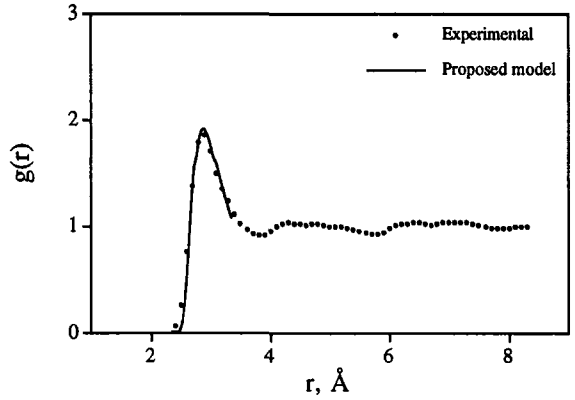

Fig. 9. Comparison of the proposed model for the first shell of RDF and the experimental data (Narten and Levy [12]) at $T = 100°C$.

them to provide extrapolated complete curves of RDF in near-critical and supercritical conditions.

$$g(x) = 1 + x^{-P_1}[P_2 - 1 - P_3] + [(x - 1 + P_3)/x]\{\exp[-P_4(x-1)]\cos[P_5(x-1)]\} \quad \text{for} \quad x > 1 \tag{47}$$

$$g(x) = P_2 \exp[-P_6(x-1)^2] \quad \text{for} \quad x < 1 \tag{48}$$

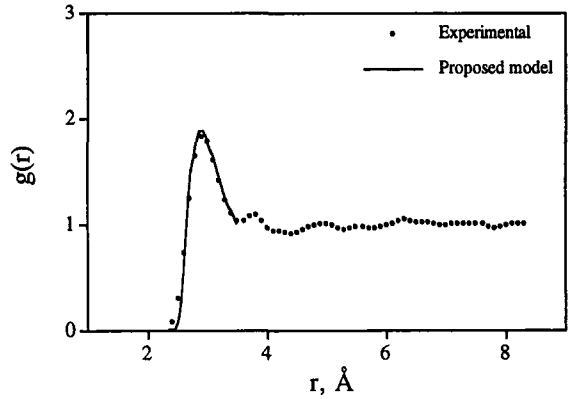

Fig. 10. Comparison of the proposed model for the first shell of RDF and the experimental data (Narten and Levy [12]) at $T = 150°C$.

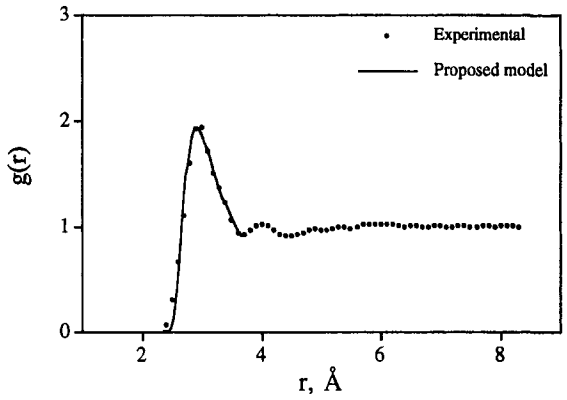

Fig. 11. Comparison of the proposed model for the first shell of RDF and the experimental data (Narten and Levy [12]) at $T = 200°C$.

where $x = r/d$, d is the contact distance, and P_i's are adjustable constants. These equations were able to reproduce the simulated RDF curves of Lennard–Jones fluids as well as their reduced internal energy and pressure in different conditions. Here we have carried out a parametrization of these equations with respect to the experimental RDF curves of Narten and Levy [12], and of the simulated curve of Chialvo and Cummings [13] at 300°C. In doing that, the following features with respect to temperature were obtained from the above data and taken into account:

(a) the trend of the height of the first peak;

(b) the behavior of the contact distance; and

(c) the value of the distance between consecutive subsequent peaks.

To extend the field of application from saturation pressure, P_{sat}, to higher pressures, we assume that features (b) and (c) depend only on the density. Moreover, the constraint was imposed that the calculated RDF curves would fit the experimental values of the isothermal compressibility, κ_T, by means of the well known equation:

$$\kappa_T = 1/(\rho kT) + 4\pi/(kT) \int_0^\infty [g(r) - 1]\, r^2\, dr \tag{49}$$

Substituting Eqs. (47) and (48) into the above equation, the following analytical expression would result for the isothermal compressibility.

$$\kappa_T = 1/(\rho kT) + 4\pi d^3/(kT)\{P_2[\gamma(0.5, P_6)/(2P_6^{0.5}) - \gamma(1, P_6)/P_6 + \gamma(1.5, P_6)/(2P_6^{1.5})] - 1/3 - (P_2\text{-}1\text{-}P_3)/(-P_1 + 3) + 2\cos[3\,\mathrm{arctg}(P_5/P_4)]/(P_4^2 + P_5^2)^{1.5} + (P_3 + 1)\cos[2\,\mathrm{arctg}(P_5/P_4)]/(P_4^2 + P_5^2) + P_3\cos[\mathrm{arctg}(P_5/P_4)]/(P_4^2 + P_5^2)^{0.5}\} \quad (50)$$

where γ is the incomplete gamma function defined by:

$$\gamma(a, \theta) \equiv \int_0^\theta X^{(a-1)} e^{-X}\, dX$$

This constraint was checked at 25°C intervals from 25 to 350°C at $P = P_{\text{sat}}$, from 100 to 400°C at $P = 0.5$ kbar, and from 175 to 475°C at $P = 1$ kbar. Accordingly, 42 constraint points have been used altogether. We utilized the experimental isothermal compressibility values reported by Helgeson and Kirkham [14]. As a result, we were able to express the seven parameters P_i as a function of temperature according to the rational equation

$$P_i = \sum_{j=1}^{6} q_{ij} t^{j-1} \Big/ \left(1 + \sum_{j=7}^{10} q_{ij} t^{j-6}\right) \quad (51)$$

where $t \equiv T/100$. The matrices of q_{ij} so obtained are reported in Table I for the three pressure values. By introducing these values in Eq. (51), Eqs. (47) and (48) reproduce the 42 values of the isothermal compressibility with an average absolute deviation of 1.1%, the maximum being 4%. Given a couple of T and P in the appropriate ranges, by interpolating each P_i parameter at the given pressure by means of the values $P_i(T, P_{\text{sat}})$, $P_i(T, 0.5\text{ kbar})$, and $P_i(T, 1\text{ kbar})$, a representation of the shape of the water RDF curve can be obtained. In other words, from these equations we can obtain a realistic picture of the RDF of water in its stable states at temperatures and pressures corresponding to those inside the polygon in Fig. 12 delimited by the dashed and solid lines.

Figures 13–15 represent comparisons between the curves produced by the first shell of RDF model, Eqs. (2) and (3), and by the extended model, Eqs. (47) and (48), at 25, 100, and 200°C; experimental data are also reported on the graphs.

Table I. Matrices of q_{ij} Defined by Eq. (51) for Parameters P_i's and d

P_i	q_{i1}	q_{i2}	q_{i3}	q_{i4}	q_{i5}	q_{i6}	q_{i7}	q_{i8}	q_{i9}	q_{i10}
					$P = P_{sat}$					
P_1	40.5443	−21.5798	4.990845	−0.452126	0.0087273	0	0	0	0	0
P_2	2.479473	−1.255942	0.173251	0	0	0	−0.5165963	0.074403	0	0
P_3	0.407978	−0.246336	0.0472025	−0.00259713	0	0	−0.855706	0275794	−0.0393497	0.0021471
P_4	−15.18289	12.16661	−3.18419	0.407711	−0.0201234	0	0	0	0	0
P_5	14.9495	−4.002514	0.873439	−0.0771996	0.00122857	0	0	0	0	0
P_6	25.6398	−23.8823	0	0	0	0	−0.508136	0.00702424	0	0
d [Å]	2.84856	−0.582133	0.026288	0	0	0	−0.204893	0.0091915	0	0
					$P = 0.5$ kbar					
P_1	56.06635	−33.38429	8.657997	−0.9992051	0.0416487	0	0	0	0	0
P_2	0.1940261	0.177105	−0.232532	0.0593095	−0.0044569	0	0.5733869	0.06271346	0.0083307	−0.001279
P_3	0.1727223	0.169313	−0.146398	0.0305596	−0.0019856	0	−0.212930	−0.1202723	0.037842	−0.00280
P_4	−56.26916	39.94523	−10.12586	1.162636	−0.0502838	0	0	0	0	0
P_5	22.92262	−9.137753	2.134173	−0.2201987	0.0078760	0	0	0	0	0
P_6	64.08279	−21.30869	0	0	0	0	−0.294835	−0.0052036	0	0
d [Å]	2.845048	−0.598729	0.035364	0	0	0	−0.2108924	0.012365	0	0
					$P = 1$ kbar					
P_1	92.85858	−57.33910	14.52609	−1.639088	0.06825348	0	0	0	0	0
P_2	2.594664	2.252273	−1.584030	0.3754453	−0.038041	0.0014187	0	0	0	0
P_3	0.0624752	0.0591594	−0.0298736	0.00332570	0	0	−0.5809955	0.1350238	−0.0152672	0.0007694
P_4	−64.41088	42.92323	−10.25177	1.104196	−0.0447506	0	0	0	0	0
P_5	22.49797	−8.292558	1.832693	−0.183401	0.00665844	0	0	0	0	0
P_6	54.06466	−17.32522	0	0	0	0	−0.2988945	0.001658190	0	0
d [Å]	2.839125	−0.483369	0.022384	0	0	0	−0.17098	0.0078265	0	0

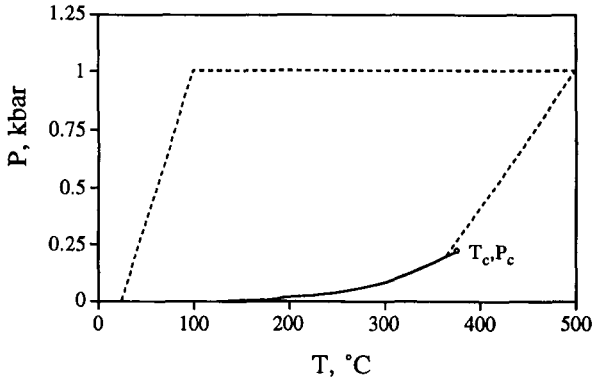

Fig. 12. Validity ranges of Eq. (50).

In order to verify the validity of the proposed model for near-critical and supercritical conditions, we have calculated the first shell of RDF for the conditions $T=300°C$, $\rho=0.72$ g·cm^{-3} and $T=400°C$, $\rho=0.66$ g·cm^{-3} for which the experimental data [15] and molecular simulation data [13] are available. Figures 16 and 17 show the corresponding comparative results for the RDF. According to these figures, there is a good general agreement among the first-shell RDF model, the extended model, the experimental results and the simulated data based on ST2 model as far as the location and height of the peak are concerned.

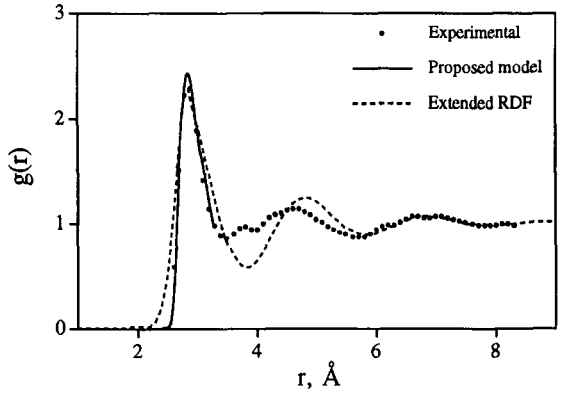

Fig. 13. Comparison of the proposed model for the first shell of RDF, extended RDF equation and the experimental data (Narten and Levy [12]) at $T=25°C$.

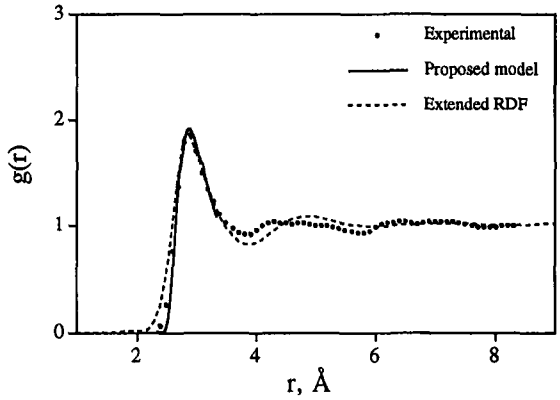

Fig. 14. Comparison of the proposed model for the first shell of RDF, extended RDF equation and the experimental data (Narten and Levy [12]) at $T = 100°C$.

In Figs. 18 and 19 we compare the results of the first-shell model with those obtained from Eqs. (47), (48), and (51) in conditions where no experimental or simulated data are available, $T = 370°C$, $\rho = 0.58\ g \cdot cm^{-3}$, and $T = 500°C$, $\rho = 0.53\ g \cdot cm^{-3}$, respectively. The agreement is satisfactory.

One of the important features of the experimental RDF data of water was reported to be the fact that as the temperature is raised from ambient

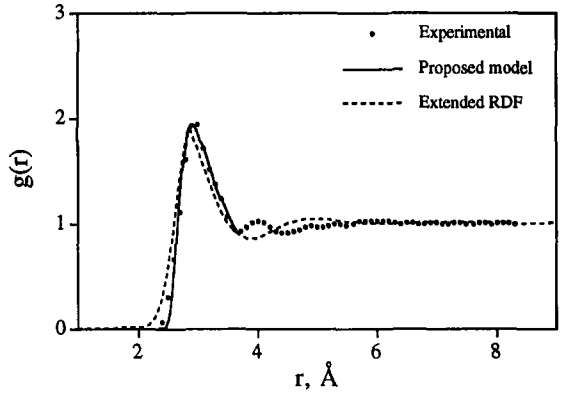

Fig. 15. Comparison of the proposed model for the first shell of RDF, extended RDF equation and the experimental data (Narten and Levy [12]) at $T = 200°C$.

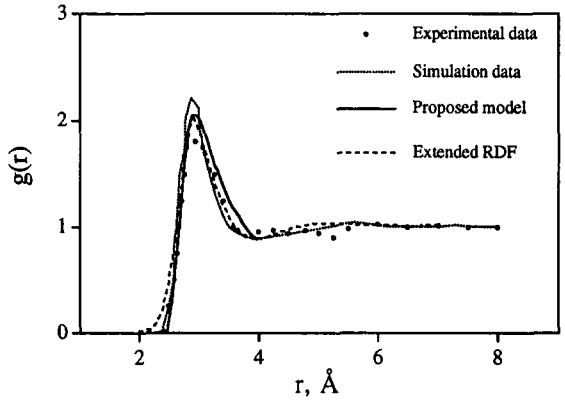

Fig. 16. Comparison of the proposed model for the first shell of RDF, the experimental data (Soper et al. [15]), the molecular simulation (Chialvo and Cummings [13]) and the extended RDF equation at $T = 300°C$.

temperature to about 170°C, the first peak diminishes a little in height, while by further increasing the temperature to the supercritical region, there is a rise in the first peak again [16]. This peculiarity of water molecules which appears in all experimental [12, 15] and simulated data [13] and is present in the treatment represented by Eqs. (47), (48), and (51), is also predicted by the proposed model.

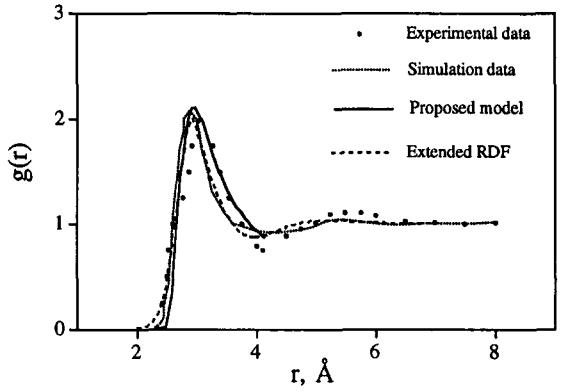

Fig. 17. Comparison of the proposed model for the first shell of RDF, the experimental data (Soper et al. [15]), the molecular simulation data (Chialvo and Cummings [13]) and the extended RDF equation at $T = 400°C$.

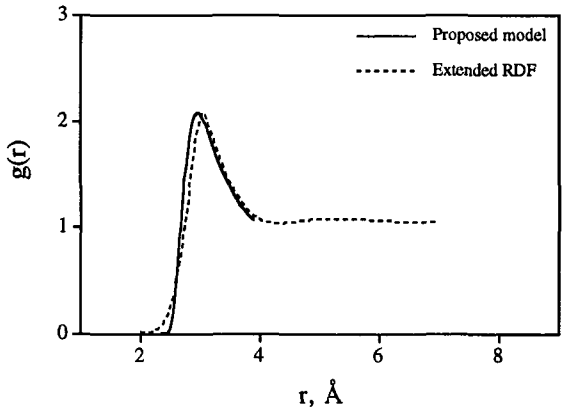

Fig. 18. Comparison of the proposed model for the first shell of RDF and the extended RDF equation at $T = 370°C$, $\rho = 0.58$.

Figures 20 to 22 represent the variations of the first peak of RDF of water at reduced temperatures ($T_r = T/T_c = T^*/T_c^*$) of 0.5, 1.0, and 1.5 and reduced densities ($\rho_r = \rho/\rho_c = \rho^*/\rho_c^*$) of 0.5, 1.0, and 2.0, respectively. In order to compare the results obtained for water with the RDF of Lennard–Jones fluids, the corresponding RDF curves for Lennard–Jones fluids at the similar conditions have been plotted on the same figures. We have chosen the critical temperature and density of Lennard–Jones fluids [17, 18]

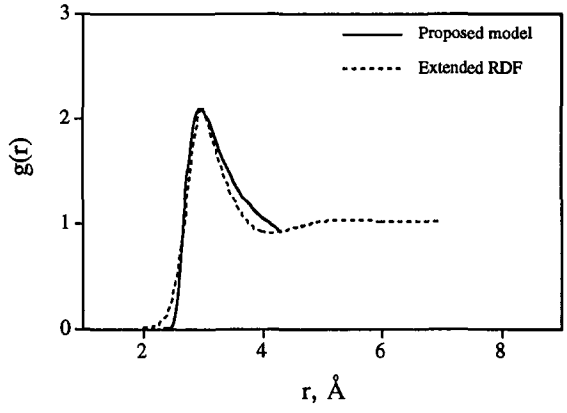

Fig. 19. Comparison of the proposed model for the first shell of RDF and the extended RDF equation at $T = 500°C$, $\rho = 0.53$.

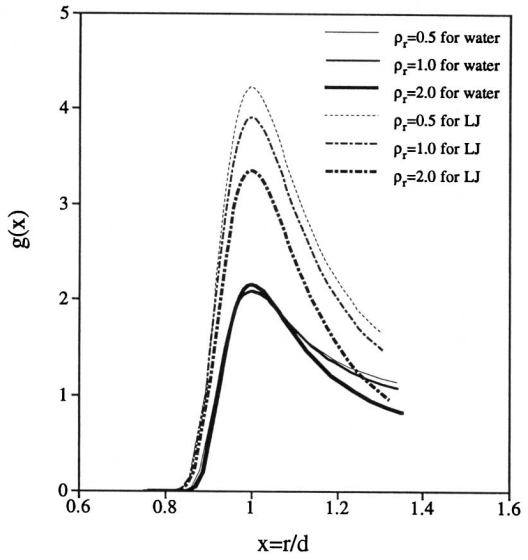

Fig. 20. Variations of the first peak of water RDF and a Lennard–Jones fluid RDF at $T_r = 0.5$.

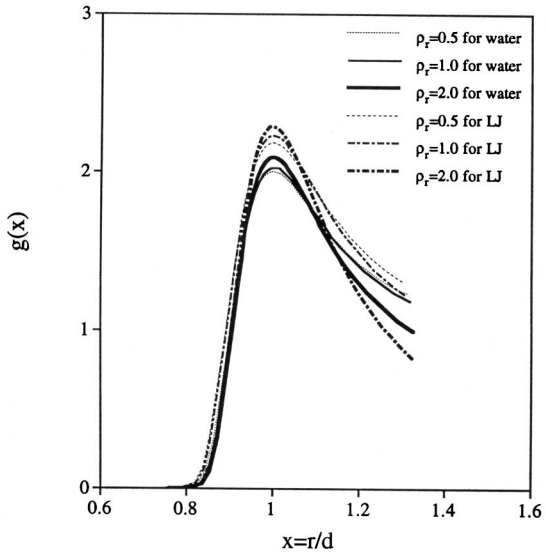

Fig. 21. Variations of the first peak of water RDF and a Lennard–Jones fluid RDF at $T_r = 1$.

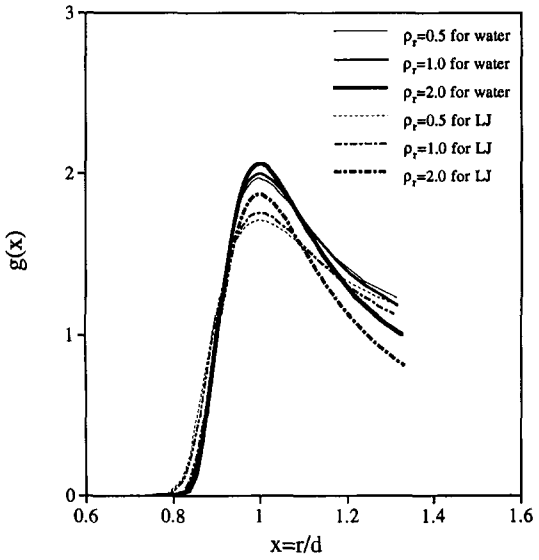

Fig. 22. Variations of the first peak of water RDF and a Lennard–Jones fluid RDF at $T_r = 1.5$.

$T_c^* = 1.31$ and $\rho_c^* = 0.31$. According to these figures, the first peaks of Lennard–Jones fluid RDFs are higher at subcritical conditions and lower at supercritical conditions than those of water.

5. SUFFICIENCY OF THE FIRST SHELL OF RDF IN CALCULATING THE ISOTHERMAL COMPRESSIBILITY

The concept of the radius of influence was proposed by Mansoori and Ely [19] for the theory of local compositions. We apply this concept to calculate the distance at which the RDF could be truncated. In all cases studied, it is shown that the radius of truncation is located inside the first shell of RDF.

By using RDF, it is possible to calculate the isothermal compressibility of a substance by applying Eq. (49). In order to make this relationship dimensionless, we define $\kappa_T^* \equiv \kappa_T \varepsilon/\sigma^3$.

$$\kappa_T^* = 1/(\rho^* T^*) + (4\pi/T^*) \int_0^\infty [\, g(y) - 1 \,]\, y^2\, dy \tag{52}$$

To calculate the isothermal compressibility using the RDF, we introduce R_κ, the radius of truncation of RDF. The integral in Eq. (52) can be written in the following form:

$$\int_0^\infty [g(y)-1]\, y^2\, dy = \int_0^{R_\kappa} [g(y)-1]\, y^2\, dy + \int_{R_\kappa}^\infty [g(y)-1]\, y^2\, dy \tag{53}$$

R_κ is chosen such that the second integral in Eq. (53) disappears, i.e.,

$$\int_{R_\kappa}^\infty [g(y)-1]\, y^2\, dy = 0 \tag{54}$$

In general, Eq. (54) has several roots for R_κ. However, we impose the constraint that R_κ has to be within the first shell of RDF. Figure 23 represents schematically the value of R_κ which gives rise to the equality of dashed areas above and below the horizontal axis to the right of R_κ. Since $g(y)$ is a function of temperature and density, R_κ is also a function of temperature and density.

Considering Eq. (54), we substitute Eq. (53) into Eq. (52).

$$\kappa_T^* = 1/(\rho^* T^*) + (4\pi/T^*) \int_0^{R_\kappa} [g(y)-1]\, y^2\, dy \tag{55}$$

Figure 24 illustrates the variations of R_κ with the temperature at P_{sat}, 0.5 and 1 kbar. In order to obtain R_κ, we have utilized the isothermal compressibility values from the experimental data reported by Helgeson and

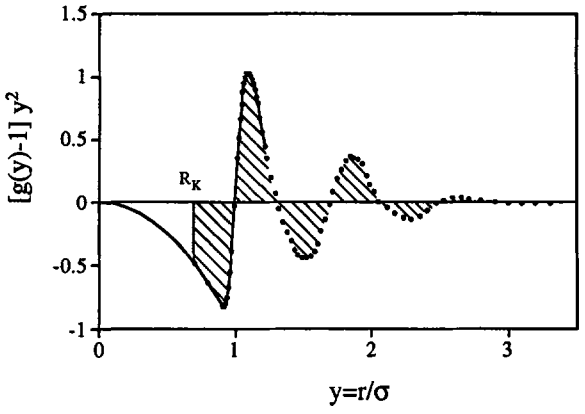

Fig. 23. Radius of truncation for the isothermal compressibility.

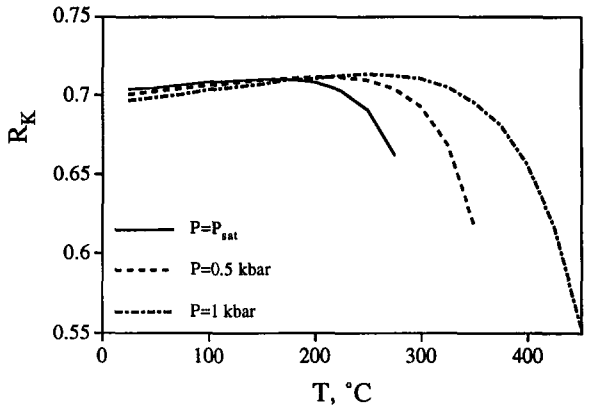

Fig. 24. Variations of the radius of truncation of RDF.

Kirkham [14]. According to Fig. 24, for all the conditions reported the radius of truncation of RDF is within the first shell.

6. CONCLUSIONS

We have extended a model for the first shell of RDF, previously developed and applied to simple fluids, to water in such a way to cover temperature and pressure ranges from ambient to supercritical conditions. This model takes into account an effective Kihara potential function by its parametrization with respect to the chain association theory and the conformal solution theory. The calculated curves of RDF compare well with subcritical experimental data and with near-critical and supercritical curves obtained either by simulation or with a semi-empirical model here devised and described. Comparison with the first peaks of RDF of Lennard–Jones fluids reveals the fact that the height of the first peak of the water RDF changes much less at subcritical and supercritical conditions than those of Lennard–Jones fluids.

ACKNOWLEDGMENTS

This research is supported in part by the U.S. National Science Foundation, Grant No. CTS-9108595 and in part by the Italian CNR.

REFERENCES

1. H. Touba and G. A. Mansoori, *Int. J. Thermophys.* **18**:1217 (1997).
2. E. Matteoli and G. A. Mansoori, *J. Chem. Phys.* **103**:4672 (1995).

3. M. S. Wertheim, *Phys. Rev. Lett.* **10**:321 (1963).
4. Y. E. Gorbaty and A. G. Kalinichev, *J. Phys. Chem.* **99**:5336 (1995).
5. T. I. Mizan, P. E. Savage, and R. M. Ziff, *J. Phys. Chem.* **100**:403 (1996).
6. K. Yamanaka, T. Yamaguchi, and H. Wakita, *J. Chem. Phys.* **101**:9830 (1994).
7. G. Nemethy and G. H. Scheraga, *J. Chem. Phys.* **36**:3382 (1962).
8. H. Touba and G. A. Mansoori, *Fluid Phase Equil.* **119**:51 (1996).
9. G. E. Walrafen, M. R. Fisher, M. S. Hokmabadi, and W. H. Yang, *J. Chem. Phys.* **85**:6970 (1986).
10. W. B. Brown, *Phil. Trans. Royal Society of London, Ser. A* **250**:175 (1957).
11. G. A. Mansoori, *Fluid Phase Equil.* **87**:1 (1993).
12. A. H. Narten and H. A. Levy, *J. Chem. Phys.* **55**:2263 (1971).
13. A. A. Chialvo and P. T. Cummings, *J. Phys. Chem.* **100**:1309 (1996).
14. H. C. Helgeson and D. H. Kirkham, *American J. Sci.* **274**:1089 (1974).
15. A. K. Soper, F. Bruni, and M. A. Ricci, *J. Chem. Phys.* **106**:247 (1997).
16. P. Postorino, R. H. Tromp, M. A. Ricci, A. K. Soper, and G. W. Neilson, *Nature* **366**:668 (1993).
17. A. Lotfi, J. Vrabec, and J. Fischer, *Mol. Phys.* **76**:1319 (1992).
18. J. K. Johnson, J. A. Zollweg, and K. E. Gubbins, *Mol. Phys.* **78**:591 (1993).
19. G. A. Mansoori and J. F. Ely, *Fluid Phase Equil.* **22**:253 (1985).